Dear Prof. Heinze,

We thank very much for your assistance with our manuscript and for accepting it for publication in Biogeosciences!

Please kindly find attached the responses with detailed specifications of the changes we introduced.

On behalf of the paper's co-authors

Best regards,

Natalia Gnatiuk

The text has a few changes. We made correction according to the following Comment:

P. 4, l. 24: use the correct abbreviations (including charges) for phosphate and nitrate;

p. 5, l. 14-15: change "nitrates, phosphates, silicates" to "nitrate, phosphate, and silicate";

p. 9, l 22.: change "didn't" to"did not".

Besides we changed the name of the biochemical reanalysis. It is very new data and we just found that it's developers have

change reanalyses name to GLOBAL_REANALYSIS_BIO_001_029.

Other changes are corrections for identified as typos and some clarification. All changes are shown in the text below.

Simulation of factors affecting *E. huxleyi* blooms in Arctic and sub-Arctic seas by CMIP5 climate models: model validation and selection

Natalia Gnatiuk[1], Iuliia Radchenko[1], Richard Davy[2], Evgeny Morozov[1], Leonid Bobylev[1]

[1]Nansen International Environmental and Remote Sensing Centre, St. Petersburg, 199034, Russia
5 [2]Nansen Environmental and Remote Sensing Center, Bergen, N-5006, Norway

Correspondence to: Natalia Gnatiuk (natalia.gnatiuk@niersc.spb.ru)

Abstract.

The observed warming in the Arctic is more than double the global average and this enhanced Arctic warming is projected to continue throughout the 21st century. This rapid warming has a wide range of impacts on polar and sub-polar marine
10 ecosystems. One of the examples of such an impact on ecosystems is that of coccolithophores, particularly *E. huxleyi*, which have expanded their range poleward during recent decades. The coccolithophore *E. huxleyi* plays an essential role in the global carbon cycle. Therefore, the assessment of future changes in coccolithophore blooms is very important.

Currently, there are a large number of climate models that give projections for various oceanographic, meteorological, and biochemical variables in the Arctic. However, individual climate models can have large biases when compared to historical
15 observations. The main goal of this research was to select an ensemble of climate models that most accurately reproduces the state of environmental variables that influence the coccolithophore *E. huxleyi* bloom over the historical period when compared to reanalysis data. We developed a novel approach for model selection to include a diverse set of measures of model skill including the spatial pattern of some variables, which had not previously included in a model selection procedure. We applied this method to each of the Arctic and sub-Arctic seas in which *E. huxleyi* blooms have been observed. Once we have selected
20 an optimal combination of climate models that most skillfully reproduce the factors which affect *E. huxleyi*, the projections of the future conditions in the Arctic from these models can be used to predict how *E. huxleyi* blooms will change in the future. Here, we present the validation of 34 CMIP5 atmosphere-ocean General Circulation Models (GCMs) over the historical period 1979-2005. Furthermore, we propose a procedure of ranking and selecting these models based on the model's skill in reproducing 10 important oceanographic, meteorological, and biochemical variables in the Arctic and sub-Arctic seas. These
25 factors include the concentration of nutrients (NO_3, PO_4, and SI), dissolved CO_2 partial pressure, pH, sea surface temperature, salinity averaged over the top 30 m, 10 m wind and surface current speed, and downwelling shortwave radiation at sea surface. The validation of the GCMs' outputs against reanalysis data includes analysis of the interannual variability, seasonal cycle, spatial biases and temporal trends of the simulated variables. In total, 60 combinations of models were selected for 10 variables over 6 study regions using the selection procedure we present here. The results show that there is no combination of models,
30 nor is there one model, that has high skill in reproducing the regional climatic-relevant features of all combinations of the considered variables in target seas. Thereby, an individual subset of models was selected according to our model selection

procedure for each combination of variable and Arctic/sub-Arctic sea. Following our selection procedure, the number of selected models in the individual subsets varied from 3 to 11.

The paper presents a comparison of the selected model subsets and the full-model ensemble of all available CMIP5 models to reanalysis data. The selected subsets of models generally show a better performance than the full-model ensemble. Therefore,
5   we conclude that within the task addressed in this study it is preferable to employ the model subsets determined through application of our procedure than the full-model ensemble.

1 Introduction

In the last three decades, the Arctic has been warming at more than twice the rate of the global average (Davy et al., 2018; Overland and Wang, 2010). This rapid warming has led to large changes in the physical environment, for example with the
10   loss of sea ice extent and volume (Dai et al., 2019; Kwok, 2018), but it has also had a large impact on the Arctic ecosystem (Hoegh-Guldberg and Bruno, 2010; Johannessen and Miles, 2011). One group of species that have been affected by Arctic warming are coccolithophores such as *Emiliania huxleyi* (hereafter *E. huxleyi)*. Reportedly, coccolithophores can affect the carbon and sulphur cycles in the surface ocean, at least within their bloom areas (Balch et al., 2016; Kondrik et al., 2018; Malin et al., 1993; Rivero-Calle et al., 2015; Winter et al., 2013). The effect of these algae on aquatic carbon chemistry results in
15   changes to the carbon fluxes between the atmosphere and ocean (Balch et al., 2016; Morozov et al., 2019; Pozdnyakov et al., 2019; Shutler et al., 2013). Additionally, they contribute to the generation of sulfate aerosols, which scatter solar radiation in the atmosphere and act as cloud condensation nuclei, enabling cloud formation (Malin and Steinke, 2004). Therefore, the coccolithophores are responsible for both warming and cooling effects on the global climate (Charlson et al., 1987; Wang et al., 2018a, 2018b).
20   Of all the coccolithophores, *E. huxleyi* is the most abundant and productive calcifying organism in the world ocean (McIntyre and Bé, 1967). It is a planktonic species growing at practically all latitudes (Brown and Yoder, 1994; Iglesias-Rodríguez et al., 2002; Moore et al., 2012) and in the eutrophic to oligotrophic marine waters (Paasche, 2001). The property of this photosynthesizing aquatic organism to produce not only organic carbon, but also calcite, i.e. particulate inorganic carbon (PIC), imparts to *E. huxleyi* a special importance for the global ocean carbon cycle, and, through intricate interactions, for CO_2
25   exchange fluxes between the ocean and atmosphere (Kondrik et al., 2019; Morozov et al., 2019; Shutler et al., 2013). Moreover, *E. huxleyi* blooms are known to *i)* affect not only the carbon but also sulphur cycles in the surface ocean, at least within bloom zones, and arguably *ii)* contribute to the generation of sulfate aerosols, which eventually enable cloud formation (Malin and Steinke, 2004). This gives *E. huxleyi* blooms a definite climatic dimension in the overall environmental impact of this phenomenon. The scale of the impact should indeed be very significant: such blooms not only release into the water huge
30   amounts of PIC, in some cases reaching nearly one million tons (Balch et al., 2016; Kondrik et al., 2018; Rivero-Calle et al., 2015), but they are very extensive typically covering marine areas in excess of many hundred thousand, sometimes up to one

million, square kilometres. Besides they occur annually across the world ocean (Brown and Yoder, 1994; Iglesias-Rodríguez et al., 2002; Moore et al., 2012). Since changes of the regional climate have influenced the ecosystems of the Arctic seas, coccolithophores, particularly *E. huxleyi*, have increasingly expanded their range into Polar waters (Henson et al., 2018; Rivero-Calle et al., 2015; Winter et al., 2013), which is thought to be due to climate warming (Fernandes, 2012; Flores et al.,

5   2010; Kondrik et al., 2017; Okada and McIntyre, 1979; Winter, 1994).

Although *E. huxleyi* cells can adapt to diverse environmental conditions, the blooms of this alga exhibit remarkable inter-annual variations in extent, intensity and localization (Balch et al., 2012; Iida et al., 2002; Kondrik et al., 2017; Morozov et al., 2013; Smyth et al., 2004). Importantly, the aforementioned spatio-temporal variations inherent in *E. huxleyi* blooms prove to be specific to individual marine environments, which indicates that *E. huxleyi* growth is generally conditioned by multiple

10   forcing factors (FFs) acting through feedback mechanisms. Reportedly, the observed spatio-temporal variations are primarily driven by changes in seawater surface temperature (SST), salinity, levels of photosynthetically active radiation (PAR) and nutrients/micronutrients availability, such as nitrate (NO_3), silicate (SI), ammonium (NH_4), phosphate (PO_4) and iron (Fe) (Iglesias-Rodríguez et al., 2002; Krumhardt et al., 2017; Lavender et al., 2008; Zondervan, 2007). However, it has been found that, in addition to the above FFs, the water column stratification and wind speed at 10 m above the surface (WS) also condition

15   the growth of *E. huxleyi:* a decrease in wind stress leads to formation of a shallow mixed layer and retaining of algal cells within the zone of high levels of PAR (Raitsos et al., 2006). The intensity of water movements in general, and specifically water advection driven by ocean surface currents (OCS), was also highly consequential in this regard (Balch et al., 2016; Pozdnyakov et al., 2019). Among the other factors affecting *E. huxleyi* blooms are carbonate chemistry variables such as CO_2 partial pressure in the water, pCO_2, and pH, which are considered to be very important (Tyrrell and Merico, 2004). There has

20   been speculation that the ongoing increase in atmospheric CO_2 should damp/inhibit the growth of coccolithophores (Rivero-Calle et al., 2015), however, this is not supported by multiple observations (Kondrik et al., 2017; Morozov et al., 2013).

As the above FFs are susceptible to climate change, these factors are expected to exert their combined influence on the intensity, spatial extent, and possibly the seasonal duration of *E. huxleyi* blooms in the future. Given that the environmental influence of this phenomenon has both climatological and biogeochemical dimensions at least on a synoptic scale, it appears

25   important to envisage how it will evolve in the mid-term future. This can be done using either biological, e.g., (Gregg et al., 2005) or statistical, e.g., (Pozdnyakov et al., 2019) *E. huxleyi* bloom models, for which the prospective tendencies in FFs are employed. In turn, the tendencies in the FFs can be obtained from climate model output.

Today atmosphere-ocean coupled climate models are state-of-the-art tools for the projection of the future climate on decadal and centennial time scales (Otero et al., 2018; Taylor et al., 2012). In particular, the modern coupled atmosphere-ocean General

30   Circulation Models (GCMs) include processes that govern the interactions between the ocean, atmosphere, land, sea ice, and the carbon cycle. The fifth phase of the Coupled Model Intercomparison Project (CMIP5) gives the opportunity to use the model output from more than 30 GCMs (Taylor et al., 2012). The GCMs provide a large number of meteorological, oceanographic and biochemical variables and so facilitate the comprehensive assessment of possible climate change impacts

on marine ecosystems in the future. However, the studies which have evaluated the CMIP model's historical simulations have shown that the model outputs have a large spread compared to natural variability (Almazroui et al., 2017; Fu et al., 2013; Gleckler et al., 2008). The full CMIP5 model ensemble has been found to be skillful at simulating continent-wide surface air temperature, and therefore useful for making robust assessments at these scales (IPCC, 2013). However, model skill at smaller

5   spatial scales, such as for the Arctic, or even for specific Arctic seas, varies considerably from region to region and for different model variables (Overland et al., 2011). Therefore, it is important to find an approach for both model evaluation (comparison with historical climate) and selection of optimal models for each specific scientific task and region that gives a skill score to each model which encompasses all the relevant model variables and properties that are important for the scientific question to be addressed.

The main goal of the paper is to quantify how well CMIP5 models reproduce the main forcing factors (FFs) that influence coccolithophore blooms in the Arctic and sub-Arctic seas. We propose a new approach for ranking and selecting CMIP5 models for their skill in capturing the historical environmental conditions in the Arctic and sub-Arctic seas (viz. the Barents, Bering, Greenland, Labrador, North and Norwegian seas). We have chosen such a specific task as a case study in order to

15   select model output to drive a model of coccolithophore blooms to predict how these will change in the future. We assume that a climate model that successfully represents the present-day conditions will also be skillful in future projections. Therefore, we select models based upon the validation of the models within the historical period.

2 Materials and method

2.1 Data

20   34 CMIP5 GCMs' outputs for the historical period 1979-2005 were used in this study. The data are freely available on the ESGF portal (https://esgf-node.llnl.gov). The list of climate models used is presented in Table 1. We analyzed five oceanographic and meteorological variables, namely the sea surface temperature (SST), salinity averaged over 0-30 m (SS_{30m}), surface wind speed at a height of 10 m (WS), ocean surface current speed (OCS), and shortwave downwelling solar radiation (SDSR); and 5 biochemical variables, namely concentration of nutrients (NO_3, PO_4, and SI), dissolved CO_2 partial pressure

25   (pCO_2), and pH. These forcing factors (FFs) are known to affect the phytoplankton life cycle in sub-polar and polar latitudes (Iglesias-Rodríguez et al., 2002; Raitsos et al., 2006; Winter et al., 2013). The analyzed CMIP5 GCMs are listed in Table 1: in total, we used outputs of 25 models for OCS, 28 for SS_{30m}, SST, and RDSR; 30 for WS; 11 for PO_4, 13 for SI and pH, 15 for pCO_2, and 16 for NO_3. The number of models employed is different and was dictated by their availability on the ESGS portal. For validation of the climate models outputs, we used atmospheric and oceanic reanalyses: (*i*) Era-Interim from the

30   European Centre for Medium-Range Weather Forecasts (https://apps.ecmwf.int) (Dee et al., 2011) for SST, WS, and RSDSR for the period from 1979 to 2005; and (*ii*) GLORYS2V4 for the from the European Copernicus Marine Environment

Monitoring Service (http://marine.copernicus.eu) SS$_{30m}$, OCS; and (*iii*) GLOBAL_REANALYSIS_BIO_001_029~~, FREEBIORYS2V4 reanalyses for biochemical variables~~ (Perruche, 2018) for 5 biochemical variables – both reanalyses from the European Copernicus Marine Environment Monitoring Service (http://marine.copernicus.eu) for the period 1993-2005. The period for verification of the employed climate models was chosen based on the length of the reanalysis data and the limitations inherent in the "historical" runs of the GCMs, which usually terminate in 2005. The selected reanalyses are widely used in the literature and have been shown to be consistent with independent observational data (Agosta et al., 2015; Dee et al., 2011; Garric et al., 2017; Geil et al., 2013).

2.2 Methods for model selection

It is well established that the method of ensemble averaging can be used to reduce systematic model biases in the individual climate models (Flato et al., 2013; Gleckler et al., 2008; Knutti et al., 2010; Pierce et al., 2009; Reichler and Kim, 2008). There are two main approaches to employing climate model ensembles: (*i*) use of the full-ensemble average data for future trends analysis (Flato et al., 2013; Gleckler et al., 2008; Knutti et al., 2010; Reichler and Kim, 2008); and (*ii*) selection of an ensemble of the models from the entire set of available climate models yielding the best fit to the observational data for a historical period (Herger et al., 2018; Knutti et al., 2010; Taylor et al., 2012). We chose the second approach for analysing the ability of GCMs to reproduce main forcing factors (FFs) that influence *E. huxleyi* bloom: nutrient concentrations (nitrate~~s~~, phosphate~~s~~, silicate~~s~~), salinity averaged over the top 30 m (SS$_{30m}$), sea surface temperature (SST), wind speed at a height of 10 m (WS), surface downwelling shortwave solar radiation (SDSR~~at the surface (RSDS~~), pH, *p*CO2, and ocean current speed (OCS).

There are many different approaches to ranking and selection climate models following validation with historical observations. For example, Agosta et al. (2015) ranked the CMIP5 models using only one statistical metric, viz, a climate prediction index (CPI), "which is widely used in climatology studies for model evaluation and weighted projections" (Connolley and Bracegirdle, 2007; Franco et al., 2011; Murphy et al., 2004). Gleckler et al. (2008) evaluated the CMIP5 models and ranked them by analy~~s~~zing the climatology of the annual cycle, inter-annual variability, and relative errors. They found that the performance of the analyzed models varied for different variables. Das et al. (2018) assessed 34 CMIP5 models using the following three criteria: the mean seasonal cycle, temporal trends, and spatial correlation. On this basis, the models were selected using a cumulative ranking approach. Fu et al. (2013) and Ruan et al. (2019) applied a score-based method using multiple criteria for the assessment of CMIP5 model performance: mean value, standard deviation, normalized root mean square error, linear correlation coefficient, Mann-Kendall test statistic Z, Sen's slope, and significance score. Further, Ruan et al. (2019) selected the top 25% ranked CMIP5 models by applying a weight criterion from 0.5 to 1.0 to the different measures. Ruan et al. (2019) reported that the introduction of multiple criteria results in fewer uncertainties in the models' performance in comparison with the respective observation data.

Having tested the approaches cited above, we developed our own methodology which combines elements from some of these. We employ the multiple criteria ranking method following Fu et al. (2013) and Ruan et al. (2019) studies but with the following

modifications: (*i*) we took into consideration the Agosta et al. (2015) climate prediction index, (*ii*) analyzed the features of spatial distribution of target variables (spatial biases and trends), (*iii*) ranked the models with the percentile method (25th, 50th, 75th) that is widely used in statistical analysis, and, finally, (*iv*) we selected the top 25% ranked CMIP5 models following Ruan et al. (2019).

5 **2.2.1 Study regions**

The target regions are six Arctic and sub-Arctic seas: the Barents, Bering, Greenland, Labrador, North and Norwegian seas, where *E. huxleyi* blooms regularly occur (Kondrik et al., 2017). As mentioned above, the reason we chose the listed seas was that, in the context of global climate change, the Arctic and sub-Arctic seas have experienced the most pronounced changes in environmental variables due to the Arctic amplification. In addition, the target seas differ in physical and geographical

10 conditions, which strongly affect their climate. While they are linked by common circulation patterns, e.g., with the warm air advection coming into the Arctic from the Atlantic Ocean, how this circulation affects the climate in a given sea is strongly affected by the local conditions. Therefore, we performed the validation and selection model procedure for each sea individually. Only specific areas within which intense growth/blooms of *E. huxleyi* frequently occur were selected in each sea according to the results obtained by Kazakov et al. (2018) based on the Ocean Colour Climate Change Initiative dataset

15 version 3.0 (https://esa-oceancolour-cci.org/) for the period from 1998 to 2016. A comparison of the area-averaged values for the entire sea and only for the region of the regular occurrence of *E. huxleyi* blooms showed a significant difference. For example, it is about 2 °C degrees among all models for SST in the Barents Sea where the *E. huxleyi* blooms cover the largest area of the sea compared to other seas. To identify the relevant study areas from a raster image that contained all blooming events over the period 1998-2016, we selected those polygons where blooms occurred for more than one 8-day period (Fig. 1).

20 For model validation we focused on sea-specific blooming periods: June-September for the Barents and Labrador seas, June-August for the Greenland Sea, May-July for the North Sea, May-August for the Norwegian Sea, and January-December for the Bering Sea (Kazakov et al., 2018). Thus, the results of the model validation can be used not only in terms of marine ecology-related issues (i.e. carbon cycle chemistry, water acidity, nutrients availability, etc.) but also for the purposes of forecasting region-specific climate-driven feedbacks between the environmental factors governing *E. huxleyi* growth.

25 **2.2.2. Model evaluation measures**

The CMIP5 climate models were validated against reanalysis data in order to assess how well they reproduce the regional features of the selected variables. The validation methodology for the GCMs' outputs included the analysis of the climatological-mean seasonal cycle, interannual variability and trends, and analysis of the spatial distribution of climatological-mean biases and trends for selected variables averaged over the blooming period in each sea.

30 a) *The seasonal cycle* was analyzed using the multi-year averaged monthly variables for all months of the year (i.e., a sample size of 12). Basic statistical measures were calculated, such as the root-mean-square deviation (RMSD), the correlation

coefficient (r), and the standard deviation (SD) (Fu et al., 2013; Gleckler et al., 2008; Kumar et al., 2015; Ruan et al., 2019). In addition, following Agosta et al. (2015) we calculated the climate prediction index (CPI), ~~for the seasonal cycle,~~ which is a ratio of the model root mean square error to the standard deviation of observation data. This model evaluation statistic weighs the simulated data against the observations and is often used to validate model output (Agosta et al., 2015; Golmohammadi et

5   al., 2014; Moriasi et al., 2007; Murphy et al., 2004; Stocker, 2004).

b) *The interannual variability* of the variables was analyzed based on monthly variables solely for blooming periods (the sample size varied according to sub-region and variables combination, e.g., a sample size for SST in the Barents Sea was 108 monthly variables from June to September during 1979-2005). The same statistical measures for analysis of the seasonal cycle were used, viz. RMSD, r, SD, and CPI.

10   c) *The spatial distribution of biases and trends* between the model outputs and the reanalysis data were calculated for temporal-averaged data in each grid point of the marine zone considered in this study.

2.2.3 Percentile ranking approach

For ranking models and selection of the model sub-set, we employed the percentile ranking approach, which is a compilation of the previously applied model ranking and the selection approaches with some modifications (see also 2.2 Methods for model

15   selection). Following Fu et al. (2013) and Ruan et al. (2019), we used multiple criteria for model selection (RMSD, r, SD). Following Agosta et al. (2015) we analyzed the climate prediction index (CPI). In addition, we ~~) and~~ considered the differences in spatial distributions of biases and trends between the model outputs and the respective reanalysis data. Further, we ranked the models based on the percentile method (25th, 50th, 75th) for each statistical measure based on the amplitude of its values. Finally, we selected the top 25% ranked CMIP5 models following Ruan et al. (2019) for each considered oceanographic, ~~and~~

20   meteorological, and biochemical variables, and the target region. Thus, for example, for a sample of 28 models, the top 25% is a sub-set of 7 models that showed the best total score (the sum of every score of statistical measures, see Tab. 2). However, if two or more models show the same score, they are all included in the selected model sub-set. Thus, the number of selected models varies from 3 to 11.

Figure 2 illustrates an example of the percentile ranking approach applied to the RMSD of SST in the Barents Sea. We divided

25   the statistical measures into 4 groups based on the amplitude of the values and assigned a score to each model according to its group: (*i*) very good models (top 25th percentile of the distribution of the statistical measures) were given a score of 3; (*ii*) good models (between 50th and 25th percentile) were given a score of 2; (*iii*) satisfactory models (between 75th and 50th percentile) were given a score of 1; and (*iv*) unsatisfactory models (more than 75th percentile) were given a score of 0. In the case of the correlation coefficient, it is vice versa, very good models with correlations scores above 0.75 were ranked with a score of 3,

30   and so forth.

For ranking models based on the differences in the spatial distribution of biases and trends between model outputs and reanalysis, we used the absolute values of the mean and the spread of the spatial variation in model biases. For example,

Figure 3 displays the box plots of spatial variability in SST biases relevant to the studied area in the Barents Sea for the blooming season (June-September) and the study period 1979-2005. The mean bias varies from -6.6 (model #20) to 1.5 °C (model #24) among the models, whereas the spread yielded by the model and that from observations has a wide spread of values from 7.3 (model #21) to 16.5 °C (model #3). Thus it can be concluded from Fig. 3 that the analysis of spatial distribution

5   of biases is very important, e.g., if we compare model #2 (ACCESS1-3) with model #3 (CanESM2), we can see that the means of these two models have a small difference (0.28 °C), while, the spread of spatial values for model #3 is much higher (by ~6 °C) than that for model #2. Application of the percentile ranking approach to model #2 (ACCESS1-3) and #3 (CanESM2) resulted in the inclusion of only the former in the model sub-set (Fig. 4).

Table 2 presents all calculated statistics that were used to rank GCMs for SST in the Barents Sea as well as the final total score

10 for each model. The spread of the total assigned scores is from 9 to 35. Based on this range we selected the top 25% of GCMs. Thus, the best model ensemble for SST for the Barents Sea is the 8-model set: ACCESS1-0; ACCESS1-3; GFDL-CM3; HadGEM2-ES; MIROC-ESM; MIROC-ESM-CHEM; MPI-ESM-LR; MPI-ESM-MR. The same procedure was performed for other target seas and variables.

3 Results and discussion

15 The results of model validation and ranking, as well as the selected CMIP5 model subsets in the Barents, Bering, Greenland, Labrador, North and Norwegian seas are presented in Fig. 4 (for 5 oceanographic, and meteorological variables), and Fig. 5 (for 5 biochemical variables). Each number in the heat maps shows the final skill score for each combination of model, variable, and sea. For each individual column, a colour gradation was applied based on our percentile ranking approach: therefore, the same numbers can have different colours on the heat maps. For example, for OCS in the Barents Sea, the spread of the final

20 model scores is from 7 to 26, whereas for SS_{30m} it is from 8 to 34. Therefore, even model #3 CanESM2 has the total score 26 for SS_{30m} (which is higher than that (25) for OCS), this model was not included in the SS_{30m} selected model sub-set and is coloured red, whereas for OSC it is included in the selected model sub-set and highlighted in green colour. The final skill scores of those models, which were included in the selected model sub-sets are marked in bold blue, and their total number is indicated at the bottom of each column.

25 Analysing the heat maps, one can conclude that there is no model ensemble, or single model, which could equally well simulate all variables over the different target seas. However, some climate models show good results for many cases, e.g., ACCESS1-3; ACCESS1-0; GFDL-CM3; GISS-E2-R; GISS-E2-R-CC; HadGEM2-AO; HadGEM2-CC; HadGEM2-ES; INMCM4; MPI-ESM-LR; MPI-ESM-MR. The models that have the lowest total scores across the majority of the target regions are CMCC-CM; FGOALS-g2; IPSL-CM5A-LR; IPSL-CM5A-MR; IPSL-CM5B-LR; MIROC5; MRI-ESM1.

30 Such heterogeneity in the ability of climate models to reproduce the climate features in different seas can be partly explained. Climate models are often tuned to adequately reproduce global processes and globally averaged values (Mauritsen et al., 2012; Schmidt et al., 2017). An insufficient number of long-time series of observations is available for model calibration, especially

for marine waters. There are also very limited observations of climate processes in the Arctic which limit model development for the Arctic environment (Vihma et al., 2014).

In order to verify our methodology, we compared selected ensemble with the full model ensemble for the time-averaged spatial distribution of biases, relative to reanalyses data for the historical period (1979/1993-2005), for each study variable in 6 target

5   seas (Fig. 6). The box plots (Fig. 6) show that the selected model ensemble mainly performs better than the full-model ensemble, i.e. mean value (red dot) located closer to the zero line (dashed). The biggest difference between these two approaches obtained for the concentration of Silicium (SI) in favour of the ranking model approach.

Analysing the box plots of the selected model ensemble (Fig. 6), the lower spread of biases is obtained for ocean current speed (OCS), salinity averaged over 30 m (SS_{30m}), and concentration of Silicium (SI). CMIP5 GCMs generally underestimate

10   RSDSR, especially over the Labrador Sea. Likewise, GCMs mainly underestimate WS except for the Labrador and Barents seas. For OCS all ensembles have a low spread of biases and its mean value located very close to zero but they have many outliers (black dots). CMIP5 GCMs in different seas show heterogeneous results – they underestimate or overestimate SST, SS_{30m}, and all biochemical variables. Also, Séférian et al. (2013) reported that CMIP5 GCMs differ enormously in biochemical variables but they show fewer biases comparing to the previous model versions (CMIP3) for wind speed. Flato et al. (2013)

15   found that CMIP5 models have higher biases (both positive and negative) for SST in polar regions, and quite large negative biases relative to other latitudes for salinity in the Arctic. Rickard et al. (2016) summarised that oceanographic variables in CMIP5 models reveal better agreement across all models compared to biochemical ones. Lavoie et al. (2013) detected that GFDL and MPI models better represent nitrate concentrations, and GFDL model best represents salinity among other considered models in the Labrador Sea. In our study, these models also selected as best for the Labrador Sea. It is quite difficult

20   to compare obtained results with other already published researches because of using different models or a various number of models in full-ensemble and study regions. Some mentioned authors apply full-model ensemble other select models with better performance, but they did not compare these two approaches as we have done.

4 Conclusions

In the paper, we presented results of validation of 34 CMIP5 models compared to ERA-Interim, GLORYS2V4 and

25   GLOBAL_REANALYSIS_BIO_001_029FREEBIORYS2V4 reanalyses for the historical period (1979/1993-2005). Besides we proposed the percentile ranking approach for selection climate model sub-sets that most accurately reproduces the state of 10 forcing factors affecting *E. huxleyi* blooms over the historical period in six Arctic and sub-Arctic seas, viz. the Barents, Bering, Labrador, Greenland, North, and Norwegian seas. In total 60 combinations of the most-skillful models were selected (10 variables and 6 target seas) based on different statistical measures: the root mean square error, correlation coefficient,

30   standard deviation, climate prediction index (CPI), spatial biases and trends. Our results show that there is no model ensemble or individual model, which could best simulate all variables across all target seas. Despite the fact that the Arctic is often considered as one single region in many studies, our results show that CMIP5 climate models do not have consistent

performance across such a large area. However, the selected model ensembles show results with smaller biases than the full-model ensemble.

The results of the percentile ranking approach proposed in this paper show better performance (mean is closer to zero) of the selected model ensemble vs. the full-model ensemble for different variables and target seas. We can conclude that it is important to include a number of different evaluation criteria when selecting the best models from an ensemble, including the spatial pattern of model biases, and that the proposed methodology is a way of improving the model selection procedure that promises a better chance to identify more skillful models for the features we are interested in.

Given that the environmental impacts of *E. huxleyi* communities are diverse and encompass both climatological and marine ecology dimensions, the established sets of CMIP5 climatological models most closely simulating the environmental conditions under which this taxon grow, open the way for envisaging how this phenomenon will further evolve in light of ongoing climate change. This can be done using *E. huxleyi* bloom model, for which the changes in the forcing factors for *E. huxlyei* blooms will be employed. Finally, although the present study has been performed for the coccolithophore *E. huxleyi* which vegetates at Arctic and sub-Arctic latitudes, the reported methodological approach is not algal-specific and can be applied to studies of other algal species composing the phytoplankton communities in the world ocean.

Author contribution

NG, RD, LB: methodology development. NG, IR: development of the paper concept. IR, NG, EM: data processing and figures producing. All authors contributed to the writing and discussion of the manuscript.

Competing interests

The authors declare that they have no conflict of interest.

Acknowledgments

We express our gratitude for the financial support of this study provided by the Russian Science Foundation (RSF) under the project 17-17-01117.

N. Gnatiuk and I. Radchenko thank Dmitry Pozdnyakov and Dmitry Kondrik for the invitation to participate in the project as well as for very useful discussions of the results obtained.

We acknowledge the members of the Coupled Model Intercomparison Project phase 5, the European Centre for Medium-Range Weather Forecasts, the European Copernicus Marine Environment Monitoring Service, and we extend our gratitude to the modelling groups specified in Table 1).

References

Agosta, C., Fettweis, X. and Datta, R.: Evaluation of the CMIP5 models in the aim of regional modelling of the Antarctic surface mass balance, Cryosph., 9, 2311–2321, 2015.

Almazroui, M., Nazrul Islam, M., Saeed, S., Alkhalaf, A. K. and Dambul, R.: Assessment of Uncertainties in Projected Temperature and Precipitation over the Arabian Peninsula Using Three Categories of Cmip5 Multimodel Ensembles, Earth Syst. Environ., 1(2), 23, doi:10.1007/s41748-017-0027-5, 2017.

Balch, W. M., Drapeau, D. T. and Bowler, B. C.: Step-changes in the physical, chemical and biological characteristics of the Gulf of Maine, as documented by the GNATS time series, Mar. Ecol. Prog. Ser., 450, 11–35, doi:10.3354/meps09555, 2012.

Balch, W. M., Bates, N. R., Lam, P. J., Twining, B. S., Rosengard, S. Z., Bowler, B. C., Drapeau, D. T., Garley, R., Lubelczyk, L. C., Mitchell, C. and Rauschenberg, S.: Factors regulating the Great Calcite Belt in the Southern Ocean and its biogeochemical significance, Global Biogeochem. Cycles, 30(8), 1124–1144, doi:10.1002/2016GB005414, 2016.

Brown, C. W. and Yoder, J. A.: Coccolithophorid blooms in the global ocean, J. Geophys. Res., 99(C4), 7467, doi:10.1029/93JC02156, 1994.

Charlson, R. J., Lovelock, J. E., Andreae, M. O. and Warren, S. G.: Oceanic phytoplankton, atmospheric sulphur, cloud albedo and climate, Nature, 326, 655–661, 1987.

Connolley, W. M. and Bracegirdle, T. J.: An Antarctic assessment of IPCC AR4 coupled models, Geophys. Res. Lett., 34(22), L22505, doi:10.1029/2007GL031648, 2007.

Dai, A., Luo, D., Song, M. and Liu, J.: Arctic amplification is caused by sea-ice loss under increasing CO 2, Nat. Commun., 10(1), doi:10.1038/s41467-018-07954-9, 2019.

Das, L., Dutta, M., Mezghani, A. and Benestad, R. E.: Use of observed temperature statistics in ranking CMIP5 model performance over the Western Himalayan Region of India, Int. J. Climatol., 38(2), 554–570, doi:10.1002/joc.5193, 2018.

Davy, R., Chen, L. and Hanna, E.: Arctic amplification metrics, Int. J. Climatol., 38(12), 4384–4394, doi:10.1002/joc.5675, 2018.

Dee, D. P., Uppala, S. M., Simmons, A. J., Berrisford, P., Poli, P., Kobayashi, S., Andrae, U., Balmaseda, M. A., Balsamo, G., Bauer, P., Bechtold, P., Beljaars, A. C. M., van de Berg, L., Bidlot, J., Bormann, N., Delsol, C., Dragani, R., Fuentes, M., Geer, A. J., Haimberger, L., Healy, S. B., Hersbach, H., Hólm, E. V., Isaksen, L., Kållberg, P., Köhler, M., Matricardi, M., McNally, A. P., Monge-Sanz, B. M., Morcrette, J.-J., Park, B.-K., Peubey, C., de Rosnay, P., Tavolato, C., Thépaut, J.-N. and Vitart, F.: The ERA-Interim reanalysis: configuration and performance of the data assimilation system, Q. J. R. Meteorol. Soc., 137(656), 553–597, doi:10.1002/qj.828, 2011.

Fernandes, M.: The Influence of Stress Conditions on Intracellular Dimethylsulphoniopropionate (DMSP) and Dimethylsulphide (DMS) Release in Emiliania huxleyi., 2012.

Flato, G., Marotzke, J., Abiodun, B., Braconnot, P., Chou, S. C., Collins, W., Cox, P., Driouech, F., Emori, S., Eyring, V., Forest, C., Gleckler, P., Guilyardi, E., Jakob, C., Kattsov, V., Reason, C. and Rummukainen, M.: Evaluation of Climate Models, in Climate Change 2013: The Physical Science Basis. Contribution of Working Group I to the Fifth Assess- ment Report of the Intergovernmental Panel on Climate Change, pp. 741–866, NY., 2013.

Flores, J. A., Colmenero-Hidalgo, E., Mejía-Molina, A. E., Baumann, K. H., H., J., L. and Rodrigues, T.: Distribution of large Emiliania huxleyi in the Central and Northeast Atlantic as a tracer of surface ocean dynamics during the last 25,000 years, Mar. Micropaleontol., 76, 53–66, 2010.

Franco, B., Fettweis, X., Erpicum, M. and Nicolay, S.: Present and future climates of the Greenland ice sheet according to the IPCC AR4 models, Clim. Dyn., 36(9–10), 1897–1918, doi:10.1007/s00382-010-0779-1, 2011.

Fu, G., Liu, Z., Charles, S. P., Xu, Z. and Yao, Z.: A score-based method for assessing the performance of GCMs: A case

study of southeastern Australia, J. Geophys. Res. Atmos., 118(10), 4154–4167, doi:10.1002/jgrd.50269, 2013.

Garric, G., Parent, L., Greiner, E., Drévillon, M., Hamon, M., Lellouche, J.-M., Régnier, C., Desportes, C., Le Galloudec, O., Bricaud, C., Drillet, Y., Hernandez, F. and Le Traon, P.-Y.: Performance and quality assessment of the global ocean eddy-permitting physical reanalysis GLORYS2V4., 19th EGU Gen. Assem. EGU2017, Proc. from Conf. held 23-28 April. 2017 Vienna, Austria., p.18776, 19, 18776, 2017.

Geil, K. L., Serra, Y. L., Zeng, X., Geil, K. L., Serra, Y. L. and Zeng, X.: Assessment of CMIP5 Model Simulations of the North American Monsoon System, J. Clim., 26(22), 8787–8801, doi:10.1175/JCLI-D-13-00044.1, 2013.

Gleckler, P. J., Taylor, K. E. and Doutriaux, C.: Performance metrics for climate models, J. Geophys. Res. Atmos., 113(D6), D06104, doi:10.1029/2007JD008972, 2008.

Golmohammadi, G., Prasher, S., Madani, A. and Rudra, R.: Evaluating Three Hydrological Distributed Watershed Models: MIKE-SHE, APEX, SWAT, Hydrology, 1(1), 20–39, doi:10.3390/hydrology1010020, 2014.

Gregg, W. W., Casey, N. W. and McClain, C. R.: Recent trends in global ocean chlorophyll, Geophys. Res. Lett., 32(3), L03606, doi:10.1029/2004GL021808, 2005.

Henson, S. A., Cole, H. S., Hopkins, J., Martin, A. P. and Yool, A.: Detection of climate change-driven trends in phytoplankton phenology, Glob. Chang. Biol., 24(1), e101–e111, doi:10.1111/gcb.13886, 2018.

Herger, N., Abramowitz, G., Knutti, R., Angélil, O., Lehmann, K. and Sanderson, B. M.: Selecting a climate model subset to optimise key ensemble properties, Earth Syst. Dyn., 9(1), 135–151, doi:10.3929/ETHZ-B-000246202, 2018.

Hoegh-Guldberg, O. and Bruno, J. F.: The Impact of Climate Change on the World's Marine Ecosystems The role of oxidative stress in differential coral bleaching View project, Science (80-.)., 328, 1523–1528, doi:10.1126/science.1189930, 2010.

Iglesias-Rodríguez, M. D., Brown, C. W., Doney, S. C., Kleypas, J., Kolber, D., Kolber, Z., Hayes, P. K. and Falkowski, P. G.: Representing key phytoplankton functional groups in ocean carbon cycle models: Coccolithophorids, Global Biogeochem. Cycles, 16(4), 47-1-47–20, doi:10.1029/2001GB001454, 2002.

Iida, T., Saitoh, S. and Miyamura, T.: Temporal and spatial variability of coccolithophore blooms in the eastern Bering Sea, 1998-2001, Prog. Oceanogr., 55, 165–175, 2002.

IPCC: Climate change 2013 the physical science basis: Working Group I contribution to the fifth assessment report of the intergovernmental panel on climate change, Cambridge University Press., 2013.

Johannessen, O. M. and Miles, M. W.: Critical vulnerabilities of marine and sea ice-based ecosystems in the high Arctic, Reg. Environ. Chang., 11(SUPPL. 1), 239–248, doi:10.1007/s10113-010-0186-5, 2011.

Kazakov, E., Kondrik, D. and Pozdnyakov, D.: Spatial data assimilation with a service-based GIS infrastructure for mapping and analysis of E. Huxleyi blooms in arctic seas, in Sixth International Conference on Remote Sensing and Geoinformation of the Environment., 2018.

Knutti, R., Furrer, R., Tebaldi, C., Cermak, J., Meehl, G. A., Knutti, R., Furrer, R., Tebaldi, C., Cermak, J. and Meehl, G. A.: Challenges in Combining Projections from Multiple Climate Models, J. Clim., 23(10), 2739–2758, doi:10.1175/2009JCLI3361.1, 2010.

Kondrik, D., Pozdnyakov, D. and Pettersson, L.: Particulate inorganic carbon production within E. huxleyi blooms in subpolar and polar seas: a satellite time series study (1998–2013), Int. J. Remote Sens., 38(22), 6179–6205, doi:10.1080/01431161.2017.1350304, 2017.

Kondrik, D., Kazakov, E. E., Pozdnyakov, D. V. and Johannessen, O. M.: Satellite evidence for enhancement of the column mixing ratio of atmospheric CO2 over E. Huxleyi blooms, Trans. Karelian Res. Cent. Russ. Acad. Sci., 9, 125–135, 2019.

Kondrik, D. V., Pozdnyakov, D. V. and Johannessen, O. M.: Satellite Evidence that E. huxleyi Phytoplankton Blooms Weaken Marine Carbon Sinks, Geophys. Res. Lett., 45(2), 846–854, doi:10.1002/2017GL076240, 2018.

Krumhardt, K. M., Lovenduski, N. S., Iglesias-Rodriguez, M. D. and Kleypas, J. A.: Coccolithophore growth and calcification in a changing ocean, Prog. Oceanogr., 159, 276–295, doi:10.1016/J.POCEAN.2017.10.007, 2017.

Kumar, D., Mishra, V. and Ganguly, A. R.: Evaluating wind extremes in CMIP5 climate models, Clim. Dyn., 45(1–2), 441–453, doi:10.1007/s00382-014-2306-2, 2015.

5 Kwok, R.: Arctic sea ice thickness, volume, and multiyear ice coverage: Losses and coupled variability (1958-2018), Environ. Res. Lett., 13(10), doi:10.1088/1748-9326/aae3ec, 2018.

Lavender, S. J., Raitsos, D. E. and Pradhan, Y.: Variations in the Phytoplankton of the North-Eastern Atlantic Ocean: From the Irish Sea to the Bay of Biscay, in Remote Sensing of the European Seas, pp. 67–78, Springer Netherlands, Dordrecht., 2008.

10 Lavoie, D., Lambert, N. and Van der Baaren, A.: Projections of future physical and biogeochemical conditions in the Northwest Atlantic from CMIP5 Global Climate Models., 2013.

Malin, G. and Steinke, M.: Coccolithophore-derived production of dimethyl sulphide, in Coccolithophores, pp. 127–164., 2004.

Malin, G., Turner, S., Liss, P., Holligan, P. and Harbour, D.: Dimethylsulphide and dimethylsulphoniopropionate in the Northeast atlantic during the summer coccolithophore bloom, Deep Sea Res. Part I Oceanogr. Res. Pap., 40(7), 1487–1508, doi:10.1016/0967-0637(93)90125-M, 1993.

Mauritsen, T., Stevens, B., Roeckner, E., Crueger, T., Esch, M., Giorgetta, M., Haak, H., Jungclaus, J., Klocke, D., Matei, D., Mikolajewicz, U., Notz, D., Pincus, R., Schmidt, H. and Tomassini, L.: Tuning the climate of a global model, J. Adv. Model. Earth Syst., 4(3), n/a-n/a, doi:10.1029/2012MS000154, 2012.

20 McIntyre, A. and Bé, A. W. H.: Modern coccolithophoridae of the atlantic ocean-I. Placoliths and cyrtoliths, Deep. Res. Oceanogr. Abstr., 14(5), doi:10.1016/0011-7471(67)90065-4, 1967.

Moore, T. S., Dowell, M. D. and Franz, B. A.: Detection of coccolithophore blooms in ocean color satellite imagery: A generalized approach for use with multiple sensors, Remote Sens. Environ., 117, 249–263, doi:10.1016/j.rse.2011.10.001, 2012.

25 Moriasi, D. N., Arnold, J. G., Liew, M. W. Van, Bingner, R. L., Harmel, R. D. and Veith, T. L.: Model evaluation guidelines for systematic quantification of accuracy in watershed simulations, Am. Soc. Agric. Biol. Eng., 50(3), 885–900, 2007.

Morozov, E., Pozdnyakov, D., Smyth, T., Sychev, V. and Grassl, H.: Space-borne study of seasonal, multi-year, and decadal phytoplankton dynamics in the Bay of Biscay, Int. J. Remote Sens., 34(4), 1297–1331, doi:10.1080/01431161.2012.718462, 2013.

30 Morozov, E., Kondrik, D., SS, C. and Pozdnyakov, D. V.: Atmospheric columnar CO2 enhancement over e. huxleyi blooms: case studies in the North Atlantic and Arctic waters, Limnol. Oceanogr., 3, 28–33, 2019.

Murphy, J. M., Sexton, D. M. H., Barnett, D. N., Jones, G. S., Webb, M. J., Collins, M. and Stainforth, D. A.: Quantification of modelling uncertainties in a large ensemble of climate change simulations, Nature, 430(7001), 768–772, doi:10.1038/nature02771, 2004.

35 Okada, H. and McIntyre, A.: Seasonal distribution of modern coccolithophores in the western North Atlantic Ocean, Mar. Biol., 54(4), 319–328, doi:10.1007/BF00395438, 1979.

Otero, N., Sillmann, J. and Butler, T.: Assessment of an extended version of the Jenkinson–Collison classification on CMIP5 models over Europe, Clim. Dyn., 50(5–6), 1559–1579, doi:10.1007/s00382-017-3705-y, 2018.

Overland, J. E. and Wang, M.: Large-scale atmospheric circulation changes are associated with the recent loss of Arctic sea ice, Tellus A Dyn. Meteorol. Oceanogr., 62(1), 1–9, doi:10.1111/j.1600-0870.2009.00421.x, 2010.

Overland, J. E., Wang, M., Bond, N. A., Walsh, J. E., Kattsov, V. M. and Chapman, W. L.: Considerations in the Selection of

Global Climate Models for Regional Climate Projections: The Arctic as a Case Study, J. Clim., 24(6), 1583–1597, doi:10.1175/2010JCLI3462.1, 2011.

Paasche, E.: A review of the coccolithophorid emiliania huxleyi (prymnesiophyceae), with particular reference to growth, coccolith formation, and calcification-photosynthesis interactions, Phycologia, 40(6), 503–529, doi:10.2216/i0031-8884-40-6-503.1, 2001.

Perruche, C.: PRODUCT USER MANUAL For the Global Ocean Biogeochemistry Hindcast GLOBAL_REANALYSIS_BIO_001_029 Issue: 1.0., 2018.

Pierce, D. W., Barnett, T. P., Santer, B. D. and Gleckler, P. J.: Selecting global climate models for regional climate change studies, Proc. Natl. Acad. Sci., 106(21), 8441–8446, 2009.

Pozdnyakov, D., Kondrik, D., Kazakov, E. and S, C.: Environmental conditions favoring coccolithophore blooms in subarctic and arctic seas: a 20-year satellite and multi-dimensional statistical study, in SPIE: Remote Sensing of the Ocean., 2019.

Raitsos, D. E., Lavender, S. J., Pradhan, Y., Tyrrell, T., Reid, P. C. and Edwards, M.: Coccolithophore bloom size variation in response to the regional environment of the subarctic North Atlantic, Limnol. Oceanogr., 51(5), 2122–2130, doi:10.4319/lo.2006.51.5.2122, 2006.

Reichler, T. and Kim, J.: How Well Do Coupled Models Simulate Today's Climate?, Bull. Am. Meteorol. Soc., 89(3), 303–312, doi:10.1175/BAMS-89-3-303, 2008.

Rickard, G. J., Behrens, E. and Chiswell, S. M.: CMIP5 earth system models with biogeochemistry: An assessment for the southwest Pacific Ocean, J. Geophys. Res. Ocean., doi:10.1002/2016JC011736, 2016.

Rivero-Calle, S., Gnanadesikan, A., Castillo, C. E. Del, Balch, W. M. and Guikema, S. D.: Multidecadal increase in North Atlantic coccolithophores and the potential role of rising CO2, Science (80-.)., 350(6267), 2015.

Ruan, Y., Liu, Z., Wang, R. and Yao, Z.: Assessing the Performance of CMIP5 GCMs for Projection of Future Temperature Change over the Lower Mekong Basin, Atmosphere (Basel)., 10(2), 93, doi:10.3390/atmos10020093, 2019.

Schmidt, G. A., Bader, D., Donner, L. J., Elsaesser, G. S., Golaz, J. C., Hannay, C., Molod, A., Neale, R. B. and Saha, S.: Practice and philosophy of climate model tuning across six US modeling centers, Geosci. Model Dev., 10(9), 3207–3223, doi:10.5194/gmd-10-3207-2017, 2017.

Séférian, R., Bopp, L., Gehlen, M., Orr, J. C., Ethé, C., Cadule, P., Aumont, O., Salas y Mélia, D., Voldoire, A. and Madec, G.: Skill assessment of three earth system models with common marine biogeochemistry, Clim. Dyn., 40(9–10), 2549–2573, doi:10.1007/s00382-012-1362-8, 2013.

Shutler, J. D., Land, P. E., Brown, C. W., Findlay, H. S., Donlon, C. J., Medland, M., Snooke, R. and Blackford, J. C.: Climate of the Past Geoscientific Instrumentation Methods and Data Systems Coccolithophore surface distributions in the North Atlantic and their modulation of the air-sea flux of CO 2 from 10 years of satellite Earth observation data, Biogeosciences, 10, 2699–2709, doi:10.5194/bg-10-2699-2013, 2013.

Smyth, T. J., Tyrrell, T. and Tarrant, B.: Time series of coccolithophore activity in the Barents Sea, from twenty years of satellite imagery, Geophys. Res. Lett., 31(11), n/a-n/a, doi:10.1029/2004GL019735, 2004.

Stocker, T. F.: Models change their tune, Nature, 430(7001), 737–738, doi:10.1038/430737a, 2004.

Taylor, K. E., Stouffer, R. J. and Meehl, G. A.: An Overview of CMIP5 and the Experiment Design, Bull. Am. Meteorol. Soc., 93(4), 485–498, doi:10.1175/BAMS-D-11-00094.1, 2012.

Tyrrell, T. and Merico, A.: Emiliania huxleyi: bloom observations and the conditions that induce them, Coccolithophores, 75–97, 2004.

Vihma, T., Pirazzini, R., Fer, I., Renfrew, I. A., Sedlar, J., Tjernström, M., Lüpkes, C., Nygård, T., Notz, D., Weiss, J., Marsan, D., Cheng, B., Birnbaum, G., Gerland, S., Chechin, D. and Gascard, J. C.: Advances in understanding and parameterization of

small-scale physical processes in the marine Arctic climate system: a review, Atmos. Chem. Phys, 14, 9403–9450, doi:10.5194/acp-14-9403-2014, 2014.

Wang, S., Maltrud, M. E., Burrows, S. M., Elliott, S. M. and Cameron-Smith, P.: Impacts of Shifts in Phytoplankton Community on Clouds and Climate via the Sulfur Cycle, Global Biogeochem. Cycles, 32(6), 1005–1026, doi:10.1029/2017GB005862, 2018a.

Wang, S., Maltrud, M., Elliott, S., Cameron-Smith, P. and Jonko, A.: Influence of dimethyl sulfide on the carbon cycle and biological production, Biogeochemistry, 138(1), 49–68, doi:10.1007/s10533-018-0430-5, 2018b.

Winter, A.: Biogeography of living coccolithophores in ocean waters, Coccolithophores, 1994.

Winter, A., Henderiks, J., Beaufort, L., Rickaby, R. E. M. and Brown, C. W.: Poleward expansion of the coccolithophore Emiliania huxleyi, J. Plankton Res., 36(2), 316–325, doi:10.1093/plankt/fbt110, 2013.

Zondervan, I.: The effects of light, macronutrients, trace metals and CO_2 on the production of calcium carbonate and organic carbon in coccolithophores-A review, Deep. Res. II, 54, 521–537, doi:10.1016/j.dsr2.2006.12.004, 2007.

journal article

Table 1. CMIP5 models used for simulation of selected variables: SST – sea surface temperature in ºC, WS – 10 m wind speed in m s^{-1}, SDSR – surface downwelling shortwave solar radiation in W m^{-2}, SS_{30m} – sea salinity (averaged over top 30 m) in PSU, OCS – surface ocean current speed in m s^{-1}, concentration of nutrients (NO_3, PO_4, and SI) in mol m^{-3}, dissolved CO_2 partial pressure (pCO$_2$) in Pa, and pH (models available for respective variable are marked as "+")

<table>
<tr><td colspan="13" align="right">Отформатированная таблица</td></tr>
</table>

Model	ID	Modelling Center (acronym, full name, and country)	Resolution (ºlon x ºlat)	SST	WS	SDSR	SS$_{30m}$	OCS	NO$_3$	PO$_4$	SI	pCO$_2$	pH
ACCESS1.0	1	CSIRO-BOM, Commonwealth Scientific and Industrial Research Organisation, Australia and Bureau of Meteorology, Australia	1.25 x 1.875	+	+	+	+	+					
ACCESS1.3	2			+	+	+	+	+					
CanESM2	3	CCCma, Canadian Centre for Climate Modelling and Analysis, Canada	2.7906 x 2.8125	+	+		+	+	+			+	+
CMCC-CM	4	CMCC, Centro euro-Mediterraneo sui Cambiamenti Climatici, Italy	0.7484 x 0.75	+	+	+	+	+					
CMCC-CMS	5		3.7111 x 3.75	+	+	+	+	+	+	+		+	+
CNRM-CM5	6	CNRM-CERFACS, Centre National de Recherches Meteorologiques, France and Centre Europeen de Recherche et Formation Avancees en Calcul Scientifique, France	1.4008 x 1.40625	+	+	+	+	+	+	+	+		
CSIRO-Mk3.6.0	7	CSIRO-QCCCE, Commonwealth Scientific and Industrial Research Organization, Australia and Queensland Climate Change Centre of Excellence, Australia	1.8653 x 1.875		+	+	+	+					
EC-EARTH	8	EC-EARTH, EC-EARTH consortium, Europe	1.1215 x 1.125	+									
GFDL-CM3	9	NOAA GFDL, National Oceanic and Atmospheric Administration, Geophysical Fluid Dynamics Laboratory, USA	2 x 2.5	+	+	+	+	+					
GFDL-ESM2G	10			+	+	+	+	+	+	+	+	+	+
GFDL-ESM2M	11			+	+	+	+	+	+	+	+	+	+
GISS-E2-H	12	NASA GISS, National Aeronautics and Space Administration, Goddard Institute for Space Studies, USA	2 x 2.5	+	+	+	+	+					
GISS-E2-H-CC	13			+	+	+	+	+	+		+	+	
GISS-E2-R	14			+	+	+	+	+					
GISS-E2-R-CC	15			+	+	+	+	+	+		+	+	
HadCM3	16	MOHC INPE, Met Office Hadley Centre, UK and Instituto Nacional de Pesquisas Espaciais, Brasil	2.5 x 3.75		+								
HadGEM2-AO	17		1.25 x 1.875	+	+	+	+	+					

Model	№	Institution	Resolution										
HadGEM2-CC	18			+	+	+	+	+	+		+	+	+
HadGEM2-ES	19			+	+	+	+	+	+		+	+	+
IPSL-CM5A-LR	20			+	+	+	+	+	+	+	+		+
IPSL-CM5A-MR	21	IPSL, Institut Pierre-Simon Laplace, France	1.8947 x 3.75	+	+	+	+	+	+	+	+		+
IPSL-CM5B-LR	22			+	+	+	+	+	+	+	+		+
MIROC5	23	MIROC, Atmosphere and Ocean Research Institute, the University of Tokyo, National Institute for Environmental Studies, and Japan Agency for Marine-Earth Science and Technology, Japan	1.4008 x 1.40625	+	+	+	+						
MIROC4h	24		0.5616 x 0.5625		+								
MIROC-ESM	25	MIROC, Japan Agency for Marine-Earth Science and Technology, Atmosphere and Ocean Research Institute, the University of Tokyo, and National Institute for Environmental Studies, Japan	2.7906 x 2.8125	+	+	+	+						+
MIROC-ESM-CHEM	26			+	+	+	+						+
MPI-ESM-LR	27	MPI-M, Max Planck Institute for Meteorology, Germany	1.8653 x 1.875	+	+	+	+	+	+	+	+	+	+
MPI-ESM-MR	28			+	+	+	+	+	+	+	+	+	+
MRI-CGCM3	29	MRI, Meteorological Research Institute, Japan	1.12148 x 1.125	+	+	+	+	+					
MRI-ESM1	30				+				+	+		+	+
NorESM1-M	31	NCC, Norwegian Climate Centre, Norway	1.8947 x 2.5	+		+	+						
NorESM1-ME	32			+		+	+	+	+	+	+	+	+
INM-CM4	33	INM, Russian Academy of Sciences Marchuk Institute of Numerical Mathematics, Russia	1.5 x 2		+	+							+
FGOALS-g2	34	LASG-CESS, Institute of Atmospheric Physics, Chinese Academy of Sciences; and Tsinghua University, China	2.7906 x 2.8125					+					
Total number of available CMIP5 models				28	30	28	28	25	16	11	13	19	13

Table 2. Results of the CMIP5 model performance for SST in the Barents Sea. Numbers in brackets indicate the models' scores.

(RMSD is the root-mean-square deviation, °C; r is the correlation coefficient between models and reanalysis; CPI is climate prediction index; $|SD_{dif}|$ is the modulus of the standard deviation difference (model minus reanalysis), °C; $|Tr_m|$ is the modulus of spatial trend mean difference (the model minus reanalysis), °C yr^{-1}; $|Tr_a|$ is the modulus of spread of spatial trends difference (the model minus reanalysis), °C yr^{-1}; $|Br_m|$ is the modulus of spatial bias mean difference (the model minus reanalysis), °C; $|Br_a|$ is the modulus of spread of spatial biases difference (the model minus reanalysis), °C).

Model acronym	ID	Seasonal cycle (averaged over the territory)				Interannual variability (averaged over the territory)				Spatial trends (Tr) and biases (Br)				Total score
		RMSD	r	CPI	$|SD_{dif}|$	RMSD	r	CPI	$|SD_{dif}|$	$|Tr_m|$	$|Tr_a|$	$|Br_m|$	$|Br_a|$	
ACCESS1-0	1	0,26(3)	0,99(2)	0,13(3)	0,08(3)	1,17(3)	0,68(3)	0,81(3)	0,02(3)	0,06(2)	0,01(3)	0,07(3)	14,7(2)	**33**
ACCESS1-3	2	0,37(3)	0,99(3)	0,19(3)	0,03(3)	1,02(3)	0,75(3)	0,71(3)	0,19(3)	0,01(3)	0,01(3)	0,57(3)	16,1(1)	**34**
CanESM2	3	1,76(2)	0,98(2)	0,88(2)	0,28(0)	2,21(2)	0,64(3)	1,54(2)	1,12(3)	0,10(1)	0,04(3)	0,85(3)	17,2(1)	24
CMCC-CM	4	5,15(0)	0,96(1)	2,58(0)	1,73(1)	7,06(0)	0,28(3)	4,90(0)	0,63(0)	0,06(2)	0,18(0)	6,64(0)	13,1(2)	9
CMCC-CMS	5	4,40(0)	0,97(2)	2,20(0)	1,34(1)	5,94(0)	0,56(3)	4,12(0)	0,59(0)	0,01(3)	0,02(3)	5,58(0)	14,1(2)	14
CNRM-CM5	6	0,64(3)	0,99(2)	0,32(3)	0,55(1)	1,59(3)	0,73(3)	1,10(3)	0,81(2)	0,08(2)	0,00(3)	0,49(3)	16,4(1)	29
EC-EARTH	7	0,41(3)	0,99(2)	0,21(3)	0,13(2)	1,43(3)	0,64(3)	0,99(3)	0,38(3)	0,13(1)	0,12(1)	0,14(3)	18,1(0)	27
GFDL-CM3	8	1,34(3)	0,99(3)	0,67(3)	0,20(3)	1,71(3)	0,80(3)	1,19(3)	0,22(3)	0,00(3)	0,09(1)	1,39(3)	11,1(3)	**34**
GFDL-ESM2G	9	3,23(1)	0,98(2)	1,62(1)	0,27(2)	3,72(1)	0,69(3)	2,58(1)	0,29(3)	0,04(3)	0,04(3)	3,46(1)	13,9(2)	23
GFDL-ESM2M	10	2,60(2)	0,99(2)	1,30(2)	0,61(3)	3,42(2)	0,68(3)	2,37(2)	0,25(2)	0,01(3)	0,08(2)	3,10(2)	15,7(1)	26
GISS-E2-H	11	3,39(1)	0,97(3)	1,70(1)	0,41(0)	4,09(1)	0,83(3)	2,84(1)	0,18(3)	0,05(2)	0,04(3)	3,86(1)	11,4(3)	25
GISS-E2-H-CC	12	3,68(1)	0,96(2)	1,84(1)	0,56(0)	4,62(1)	0,72(3)	3,20(1)	0,12(2)	0,03(3)	0,02(3)	4,36(1)	10,8(3)	24
GISS-E2-R	13	3,34(1)	0,96(2)	1,67(1)	0,04(1)	3,83(1)	0,72(3)	2,66(1)	0,84(3)	0,05(2)	0,07(2)	3,34(1)	15,1(2)	20
GISS-E2-R-CC	14	3,38(1)	0,96(2)	1,69(1)	0,07(1)	3,78(1)	0,75(3)	2,62(1)	0,83(3)	0,03(3)	0,05(2)	3,29(2)	13,6(2)	22
HadGEM2-AO	15	1,28(3)	0,99(2)	0,64(3)	0,01(3)	1,51(3)	0,73(3)	1,05(3)	0,13(3)	0,02(3)	0,05(2)	1,33(3)	19,8(0)	31
HadGEM2-CC	16	1,70(2)	0,99(2)	0,85(2)	0,16(2)	2,34(2)	0,62(3)	1,62(2)	0,35(3)	0,05(2)	0,05(2)	1,66(3)	19,1(0)	25
HadGEM2-ES	17	0,30(3)	0,99(3)	0,15(3)	0,08(3)	0,98(3)	0,77(3)	0,68(3)	0,00(3)	0,05(2)	0,04(3)	0,09(3)	17,5(1)	**33**
IPSL-CM5A-LR	18	3,66(1)	0,98(2)	1,83(1)	0,31(3)	4,59(1)	0,70(3)	3,19(1)	0,18(3)	0,01(3)	0,03(3)	4,32(1)	18,4(0)	22
IPSL-CM5A-MR	19	2,22(2)	0,99(2)	1,11(2)	0,67(1)	2,57(2)	0,73(3)	1,78(2)	0,80(2)	0,06(2)	0,05(2)	1,91(2)	16,0(1)	23
IPSL-CM5B-LR	20	5,03(0)	0,96(1)	2,52(0)	1,71(1)	6,90(0)	0,36(3)	4,79(0)	0,69(0)	0,00(3)	0,03(3)	6,51(0)	17,6(0)	11
MIROC-ESM	21	1,40(3)	0,99(3)	0,70(3)	0,04(3)	1,63(3)	0,82(3)	1,13(3)	0,06(3)	0,01(3)	0,08(2)	1,51(3)	11,8(3)	**35**
MIROC-ESM-CHEM	22	0,97(3)	0,99(3)	0,49(3)	0,05(3)	1,34(3)	0,82(3)	0,93(3)	0,13(3)	0,07(2)	0,05(3)	1,08(3)	15,1(2)	**34**
MIROC5	23	2,42(0)	0,98(2)	1,21(0)	0,51(1)	5,69(2)	0,51(3)	3,95(2)	0,64(2)	0,18(0)	0,08(2)	5,14(0)	19,8(0)	14
MPI-ESM-LR	24	1,27(3)	0,99(3)	0,63(3)	0,04(3)	1,54(3)	0,81(3)	1,07(3)	0,21(3)	0,02(3)	0,04(3)	1,33(3)	16,3(1)	**34**
MPI-ESM-MR	25	0,91(3)	0,99(2)	0,45(3)	0,05(3)	1,47(3)	0,71(3)	1,02(3)	0,11(3)	0,05(2)	0,04(3)	0,96(3)	17,2(1)	**32**
MRI-CGCM3	26	2,88(2)	0,99(3)	1,44(0)	0,08(3)	2,54(1)	0,82(3)	1,77(1)	0,34(3)	0,00(3)	0,07(2)	2,30(2)	11,9(3)	27
NorESM1-M	27	1,53(2)	0,99(2)	0,77(2)	0,76(2)	2,56(2)	0,64(2)	1,78(2)	0,31(2)	0,05(2)	0,07(2)	2,33(2)	13,7(2)	25
NorESM1-ME	28	1,72(2)	0,99(2)	0,86(2)	0,78(2)	2,79(2)	0,57(3)	1,94(2)	0,39(2)	0,02(3)	0,02(3)	2,58(2)	15,0(2)	27
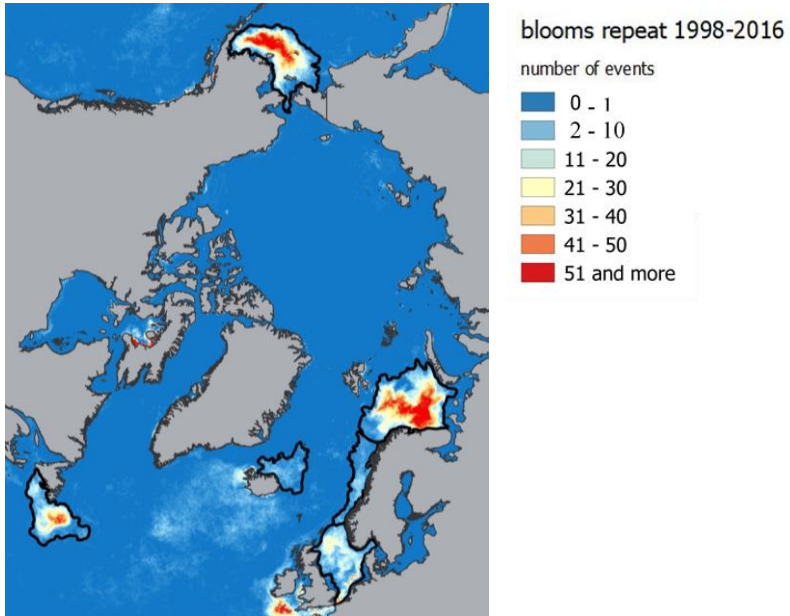
Figure 1: **Spatial distribution of** *E. huxleyi* **blooms occurrence based on the Ocean Colour Climate Change Initiative dataset version 3.0** (Kazakov et al., 2018) **for the Barents, Bering, Labrador, Greenland, North, and Norwegian seas. Black lines confine the territories where blooms occurred more than one 8-day period and show target sea areas.**
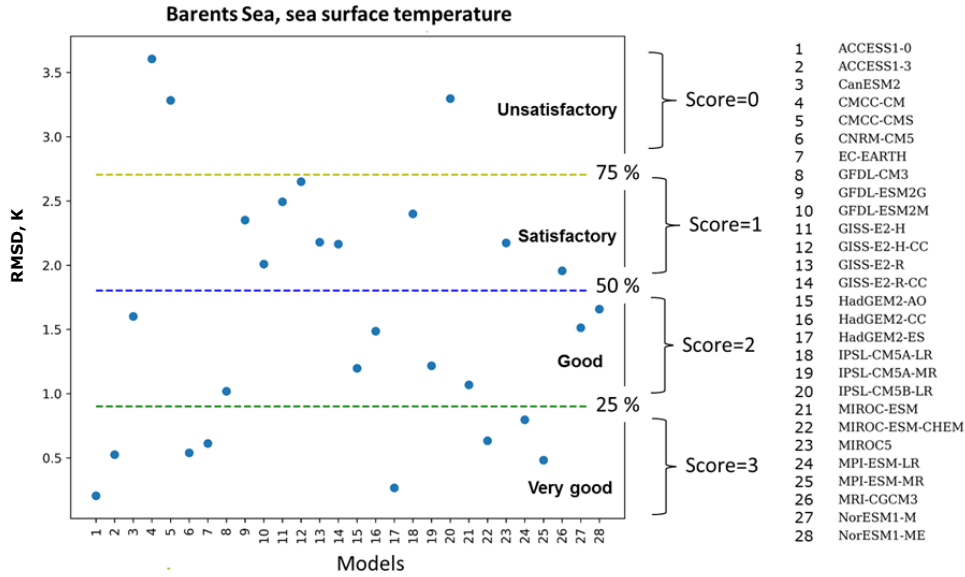
Figure 2: A schematic representation of the percentile ranking approach: division of RMSD values distribution of 28 models into four groups that are limited by 25th, 50th, and 75th percentiles and the relative assignment of scores from 3 to 0 to each group accordingly – very good, good, satisfactory and unsatisfactory.
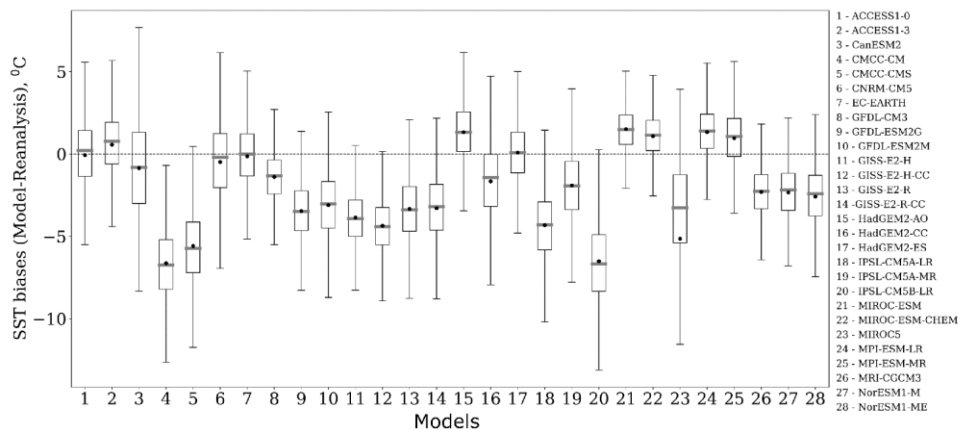
Figure 3: Box plots of the spatial variability of SST biases (°C), which are calculated as the difference between the model and reanalysis data in the Barents Sea for *E. huxleyi* bloom season over the period from 1979 to 2005. Each box spreads from the lower quartile Q1 to the upper quartile Q3 of biases, the greay lines represent the medians. The dots show mean values. The lower "whiskers" are represented as Q1-1.5 standard deviation and the upper "whiskers" are represented as Q3+1.5 standard deviation.
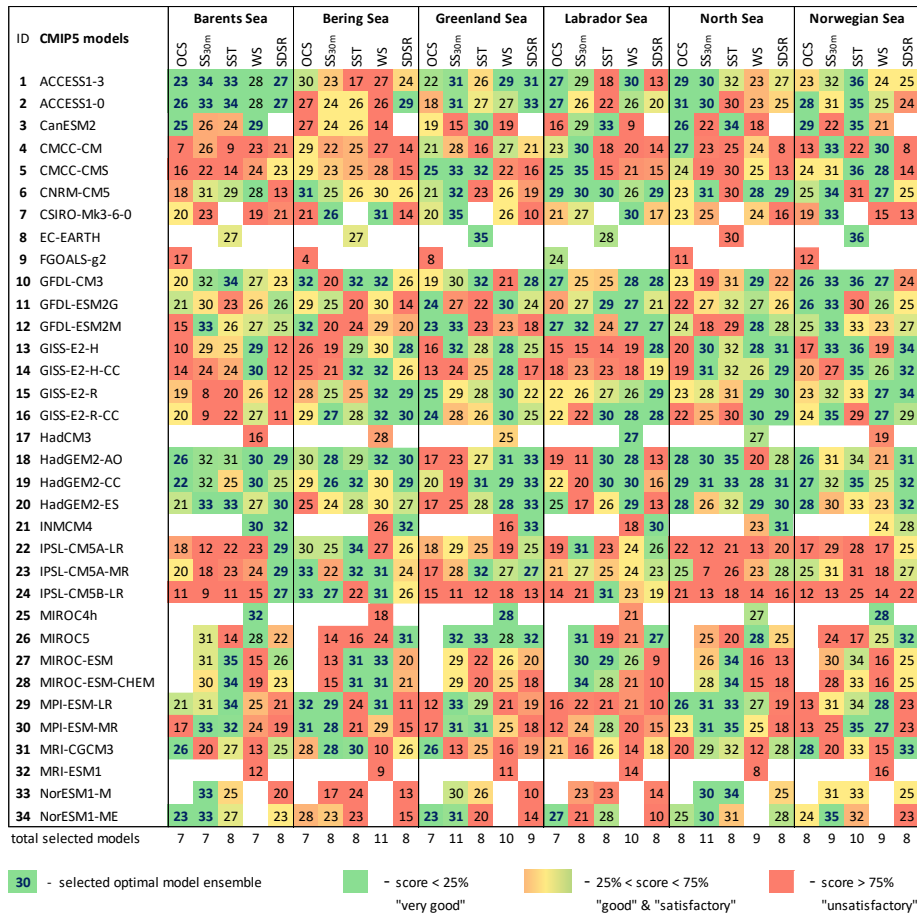
Figure 4. Heat map with the final model scores obtained using the percentile ranking approach for the 5 oceanographic and meteorological variables (sea surface temperature (SST), salinity averaged over 0-30 m (SS$_{30m}$), surface wind speed at 10 m (WS), ocean surface current speed (OCS), and surface shortwave downwelling solar radiation (SDSR) for the Barents, Bering, Greenland, Labrador, North, and Norwegian seas based on different statistical measures (Fig. 2, Tab. 2). The white areas indicate a lack of model output for historical and RCP projections (RCP4.5, RCP8.5) in open data sources.

ID	CMIP5 models	Barents Sea					Bering Sea					Greenland Sea					Labrador Sea					North Sea					Norwegian Sea				
		OCS	SS$_{30m}$	SST	WS	SDSR	OCS	SS$_{30m}$	SST	WS	SDSR	OCS	SS$_{30m}$	SST	WS	SDSR	OCS	SS$_{30m}$	SST	WS	SDSR	OCS	SS$_{30m}$	SST	WS	SDSR	OCS	SS$_{30m}$	SST	WS	SDSR
1	ACCESS1-3	23	34	33	28	27	30	23	17	27	24	22	31	26	29	31	27	29	18	30	13	29	30	32	23	27	23	32	36	24	25
2	ACCESS1-0	26	33	34	28	27	27	24	26	26	29	18	31	27	27	33	27	26	22	26	20	31	30	30	23	25	28	31	35	25	24
3	CanESM2	25	26	24	29		27	24	26	14		19	15	30	19		16	29	33	9		26	22	34	18		29	22	35	21	
4	CMCC-CM	7	26	9	23	21	29	22	25	27	14	21	28	16	27	21	23	30	18	20	14	27	23	25	24	8	13	33	22	30	8
5	CMCC-CMS	16	22	14	24	23	29	23	25	28	15	25	33	32	22	16	25	35	15	21	15	24	19	30	25	13	24	31	36	28	14
6	CNRM-CM5	18	31	29	28	13	31	25	26	30	26	21	32	23	26	19	29	30	30	26	29	23	31	30	28	29	25	34	31	27	25
7	CSIRO-Mk3-6-0	20	23		19	21	21	26		31	14	20	35		26	10	21	27		30	17	23	25		24	16	16	33		15	13
8	EC-EARTH			27					27					35					28					30					36		
9	FGOALS-g2	17					4					8					24					11					12				
10	GFDL-CM3	20	32	34	27	23	32	20	32	32	26	19	30	32	21	28	27	25	25	28	28	23	19	31	29	22	26	33	36	27	24
11	GFDL-ESM2G	21	30	23	26	26	29	25	20	30	14	24	27	22	30	24	20	27	29	27	21	22	27	32	27	26	26	33	30	26	25
12	GFDL-ESM2M	15	33	26	27	25	32	20	24	29	20	23	33	23	23	18	27	32	24	27	27	25	18	29	28	25	28	33	33	23	27
13	GISS-E2-H	10	29	25	29	12	26	19	29	30	28	16	32	28	28	25	15	15	14	19	28	20	30	32	28	31	17	33	36	19	34
14	GISS-E2-H-CC	14	24	24	30	12	25	21	32	32	28	13	24	25	28	17	18	23	23	18	19	19	31	32	26	29	20	27	35	26	32
15	GISS-E2-R	19	8	20	26	12	28	25	25	32	29	25	29	28	30	22	22	26	27	26	29	23	28	31	29	30	23	32	33	27	34
16	GISS-E2-R-CC	20	9	22	27	11	29	27	28	32	30	24	28	26	30	25	22	22	30	28	28	22	25	30	30	29	24	35	29	27	29
17	HadCM3			16					28					25					27					27					19		
18	HadGEM2-AO	26	32	31	30	29	30	28	29	32	30	17	23	27	31	33	19	11	30	28	13	28	30	35	20	28	26	31	34	21	31
19	HadGEM2-CC	22	32	25	30	25	29	26	32	30	29	20	19	31	29	32	16	29	30	30	16	29	31	32	28	31	27	32	35	25	32
20	HadGEM2-ES	21	33	33	27	30	25	24	28	30	27	17	25	28	28	33	25	17	26	29	13	28	26	32	29	30	28	30	33	23	32
21	INMCM4				30	32	26				32			16		33		18		30					23	31				24	28
22	IPSL-CM5A-LR	18	12	22	23	29	30	25	34	27	26	18	29	25	19	25	19	31	23	24	26	22	12	21	13	20	17	29	28	17	25
23	IPSL-CM5A-MR	20	18	23	24	29	33	22	32	31	24	17	28	32	27	27	21	27	25	24	23	25	7	26	23	28	25	31	31	18	27
24	IPSL-CM5B-LR	11	9	11	15	27	33	27	22	31	26	15	11	12	18	13	21	31	23	19	13	21	13	18	14	16	12	13	25	14	22
25	MIROC4h				32					18					28					21					27					28	
26	MIROC5		31	14	28	22		14	16	24	31		32	33	28	32		31	19	21	27		25	20	28	25		24	17	25	32
27	MIROC-ESM		31	35	15	26		13	31	33	20		29	22	26	20		30	29	26	9		26	34	16	13		30	34	16	25
28	MIROC-ESM-CHEM		30	34	19	23		15	31	31	21		29	20	25	18		28	34	15	18		28	33	16	25		28	33	16	25
29	MPI-ESM-LR	21	31	34	25	21	32	29	24	31	11	12	33	29	21	19	16	22	21	33	27	26	31	33	27	19	13	31	34	28	23
30	MPI-ESM-MR	17	33	32	24	19	31	28	21	29	15	17	31	31	25	18	12	24	28	20	15	23	31	35	25	18	13	35	35	27	23
31	MRI-CGCM3	26	20	27	13	25	28	28	30	10	26	26	13	25	16	19	21	16	26	14	18	20	29	32	12	28	28	20	33	15	33
32	MRI-ESM1			12					9					11					14					8					16		
33	NorESM1-M		33	25	20				17	24			30	26		10	23	23			14		30	34		25		31	33		
34	NorESM1-ME	23	33	27		23	28	23	23		15	23	31	20		14	27	21	28		10	25	30	31		28	24	35	32		23
	total selected models	7	7	8	7	8	7	8	8	11	8	7	11	8	10	9	7	8	8	10	8	8	11	8	9	8	8	9	9	10	9

30 – selected optimal model ensemble

– score < 25% "very good"
– 25% < score < 75% "good" & "satisfactory"
– score > 75% "unsatisfactory"

ID	CMIP5 models	Barents					Bering					Greenland					Labrador					North					Norwegian				
		NO₃	PO₄	SI	pH	pCO₂	NO₃	PO₄	SI	pH	pCO₂	NO₃	PO₄	SI	pH	pCO₂	NO₃	PO₄	SI	pH	pCO₂	NO₃	PO₄	SI	pH	pCO₂	NO₃	PO₄	SI	pH	pCO₂
1	CanESM2	14			22	26	13			11	23	12			27	29	14			22	15	20			28	21	16			23	28
2	CMCC-CESM	9	12		9	25	13	3		10	20	7	13		6	13	14	5		6	13	23	6		9	15	9	17		6	14
3	CNRM-CM5	5	10	30			19	32	20			10	6	29			5	4	27			9	14	22			6	8	28		
4	GFDL-ESM2G	27	22	18	24	29	21	32	24	18	30	17	16	24	9	18	17	17	28	25	20	23	22	28	27	24	8	7	21	18	21
5	GFDL-ESM2M	23	21	26	12	23	18	34	25	13	29	12	11	26	5	16	14	10	28	17	15	10	21	21	23	16	16	21	25	10	10
6	GISS-E2-H-CC	10	26		5		9		21		22	9		27		6	16		26			24			23	12	12		31		16
7	GISS-E2-R-CC	11	29		11		11		22		7	10		25		15	17		26		30	24			20	20	15		26		25
8	HadGEM2-CC	12	8	20	26		5		11	8	24	9		8	20	27	17		11	18	14	22		12	23	15	12		15	12	16
9	HadGEM2-ES	12		14	19	27	4		12	7	25	10		8	24	32	17		15	23	17	22		12	25	17	13		15	15	20
10	inmcm4					22					26					27				14						21					11
11	IPSL-CM5A-LR	15	16	27	20		10	33	22	17		11	11	28	11		18	3	26	14		24	18	26	21		18	9	30	18	
12	IPSL-CM5A-MR	18	19	29	19		17	35	21	19		12	9	28	23		16	5	29	17		24	20	27	26		20	15	30	17	
13	IPSL-CM5B-LR	19	15	27	21		10	33	20	13		11	7	29	14		11	3	27	15		21	13	23	17		16	10	29	20	
14	MIROC-ESM					30					28					19				18						19					18
15	MIROC-ESM-CHEM					30					27					21				18					14						19
16	MPI-ESM-LR	23	24	28	27	33	8	32	23	10	24	19	17	23	15	26	17	12	34	23	24	27	27	26	30	30	22	24	32	17	22
17	MPI-ESM-MR	20	25	27	29	32	7	33	26	14	25	17	12	27	16	26	18	9	33	23	24	27	23	25	30	33	22	19	30	18	25
18	MRI-ESM1	18	14		19	26	13	32		6	26	22	22		27	27	20	19		16	23	26	10		28	20	21	13		18	18
19	NorESM1-ME	12	10	22	22	28	7	32	12	18	30	7	8	21	9	19	9	14	13	11	15	17	13	26	26	26	15	14	23	7	19
	total selected models	4	3	3	3	4	4	5	3	3	4	4	3	4	3	5	8	3	3	4	4	7	3	5	4	4	4	3	5	6	4

30 – selected optimal model ensemble   ■ – score < 25% "very good"   ■ – 25% < score < 75% "good" & "satisfactory"   ■ – score > 75% "unsatisfactory"

Figure 5: Heat map with the final model scores obtained using the percentile ranking approach for the 5 biochemical variables (concentration of nutrients (NO₃, PO₄, and SI), dissolved CO₂ partial pressure (pCO₂), and pH) for the Barents, Bering, Greenland, Labrador, North, and Norwegian seas based on different statistical measures (Fig. 2, Tab. 2). The white areas indicate a lack of model output for historical and RCP projections (RCP4.5, RCP8.5) in open data sources.
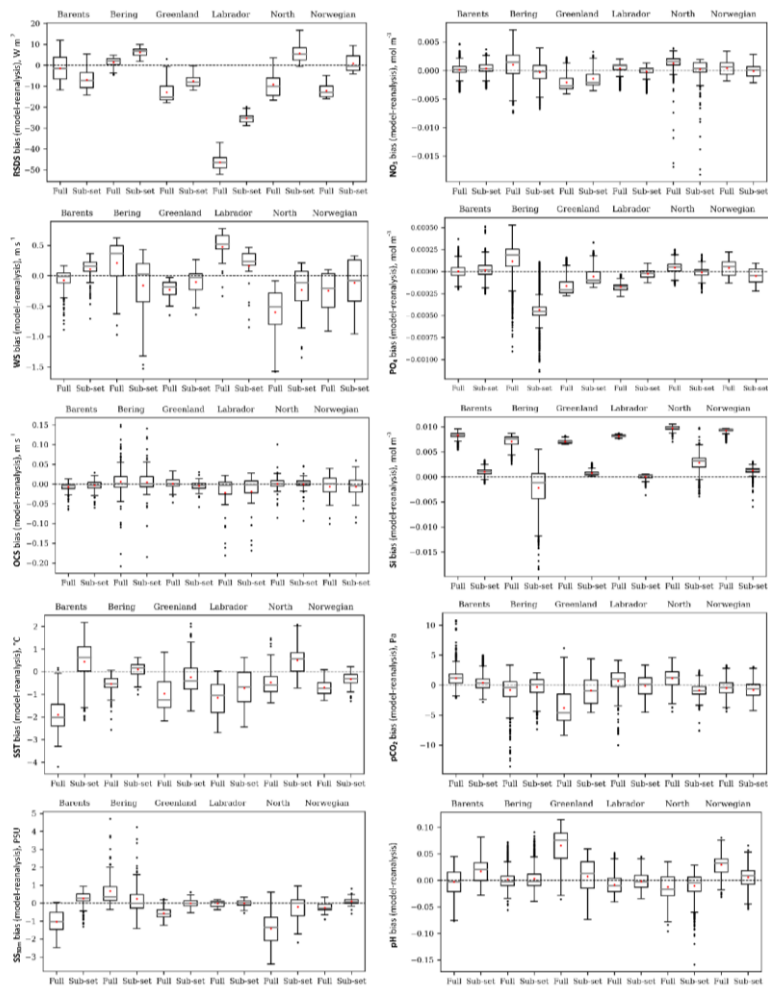
Figure 6: **Box plots of the spatial distribution of biases (model ensemble minus reanalyses) of 5 oceanographic and meteorological (left), and 5 biochemical variables (right): sea surface temperature (SST), salinity averaged over 0-30 m (SS$_{30m}$), surface wind speed at 10 m (WS), ocean surface current speed (OCS), surface shortwave downwelling solar radiation (SDSR), concentration of nutrients**

(NO₃, PO₄, and SI), dissolved CO_2 partial pressure ($p$$CO_2$), and pH for the Barents, Bering, Greenland, Labrador, North, and Norwegian seas averaged over the study period for comparison of full and selected model ensembles.